Supplementary Table 1 | Binding constants derived from ensemble fluorescence measurements

	E1A-TAZ2 (K_1 / nM)[a]		E1A-pRb (K_2 / nM)[a]	
	Direct Titration	Competition	Direct Titration	Competition
$E1A_{N}$ (1-36; 36C) 	50 ± 5	45 ± 20[1]	> 1000	*n.d.*
$E1A_{CR2}$ (106-139; 137C) 	1040 ± 200[b]	*n.d.*	110 ± 30	90 ± 30[3]
$E1A_{CR1}$ (27-105; 88C) 	< 25	*n.d.*	390 ± 50	280 ± 20[4]
$E1A_{N\text{-}CR1}$ (1-105; 88C) 	< 25	*n.d.*	450 ± 70[b]	*n.d.*
$E1A_{CR1\text{-}CR2}$ (27-139; 88C) 	< 25	5 ± 1[2]	< 25	12 ± 3[5]
$E1A_{N\text{-}CR1\text{-}CR2}$ (1-139; 88C) 	< 25	*n.r.*	< 25	*n.r.*

[a] Unless stated otherwise, the reported binding constants are the average of two independent experiments, and the reported errors are standard deviations (see Supplementary Figure 2).
[b] Derived from single measurement; errors obtained from nonlinear least-squares (NLS) fitting
n.d. Not determined
n.r. Not reliable due to protein aggregation
[1-5] Derived assuming dissociation constant (K_d) values of 50, 13, 112, 385 and 25 nM, respectively, for the direct titration measurements

Supplementary Table 2 | Binding constants derived from single-molecule FRET experiments

	E1A-pRb (K_2 / nM)[a]	E1A-TAZ2 (K_1 / nM)[a]	pRb-E1A-TAZ2 ($K_{1'}$ / nM)[a]		
			+ 0.25 μM pRb	+ 1 μM pRb	+ 1.5 μM pRb
$E1A_{CR1}$ (27-105; 36C88C)	390 ± 50[b]	11.7 ± 0.4	*n.d.*	34 ± 6	40 ± 4
$E1A_{N\text{-}CR1}$ (1-105; 36C88C)	450 ± 70[b]	3.2 ± 0.5	4.5 ± 1.2	1.5 ± 0.3	*n.d.*
$E1A_{CR1\text{-}CR2}$ (27-139; 36C88C)	4.1 ± 0.4	7.5 ± 1.0	11.3 ± 4.4	18 ± 6	*n.d.*
$E1A_{N\text{-}CR1\text{-}CR2}$ (1-139; 36C88C)	4.5 ± 0.4	1.6 ± 0.3	4.0 ± 1.3	*n.d.*	*n.d.*
$E1A_{CR1\text{-}CR2}$ (27-139; -3C111C)	13.0 ± 2.6	18.2 ± 2.5	37 ± 31	*n.d.*	*n.d.*
$E1A_{N\text{-}CR1\text{-}CR2}$ (1-139; -3C111C)	10 ± 2	10.2 ± 1.1	6.3 ± 1.5	*n.d.*	*n.d.*
$E1A_{CR1\text{-}CR2}$ (27-139; 36C137C)	8.2 ± 0.7	2.6 ± 0.5	*n.d.*[c]	*n.d.*	*n.d.*
$E1A_{N\text{-}CR1\text{-}CR2}$ (1-139; 36C137C)	13.6 ± 0.5	2.3 ± 0.5	*n.d.*[c]	*n.d.*	*n.d.*

[a] Unless stated otherwise, K_d errors are average fitting errors between the NLS fits of the free and bound species titration data (see Supplementary Figures 3-6 and Methods).
[b] Derived from ensemble anisotropy measurements (Supplementary Table 1)
[c] Could not be determined due to very similar E_{FRET} signals for the E1A-pRb, E1A-TAZ2 and E1A-TAZ2-pRb complexes (Supplementary Table 3)
n.d. Not determined because lower pRb concentrations are sufficient for saturation

Supplementary Table 3 | E_{FRET} characteristics of different E1A dual-labeled constructs

	FRET Efficiencies*			
	E1A	E1A-pRb	E1A-TAZ2	pRb-E1A-TAZ2
$E1A_{CR1}$ (27-105; 36C88C)	0.46 ± 0.02	0.43 ± 0.01	0.90 ± 0.01	0.87 ± 0.04
$E1A_{N\text{-}CR1}$ (1-105; 36C88C)	0.45 ± 0.01	0.45 ± 0.01	0.83 ± 0.01	0.82 ± 0.01
$E1A_{CR1\text{-}CR2}$ (27-139; 36C88C)	0.47 ± 0.01	0.67 ± 0.01	0.87 ± 0.02	0.91 ± 0.01
$E1A_{N\text{-}CR1\text{-}CR2}$ (1-139; 36C88C)	0.44 ± 0.01	0.66 ± 0.01	0.83 ± 0.01	0.87 ± 0.01
$E1A_{CR1\text{-}CR2}$ (27-139; -3C111C)	0.29 ± 0.01	0.67 ± 0.01	0.76 ± 0.01	0.76 ± 0.01
$E1A_{N\text{-}CR1\text{-}CR2}$ (1-139; -3C111C)	0.23 ± 0.01	0.41 ± 0.01	0.73 ± 0.01	0.73 ± 0.03
$E1A_{CR1\text{-}CR2}$ (27-139; 36C137C)	0.24 ± 0.01	0.82 ± 0.01	0.86 ± 0.01	0.80 ± 0.01
$E1A_{N\text{-}CR1\text{-}CR2}$ (1-139; 36C137C)	0.23 ± 0.01	0.80 ± 0.01	0.81 ± 0.01	*n.d.*

n.d. Could not be determined
* Errors reported are the standard deviation of multiple measurements

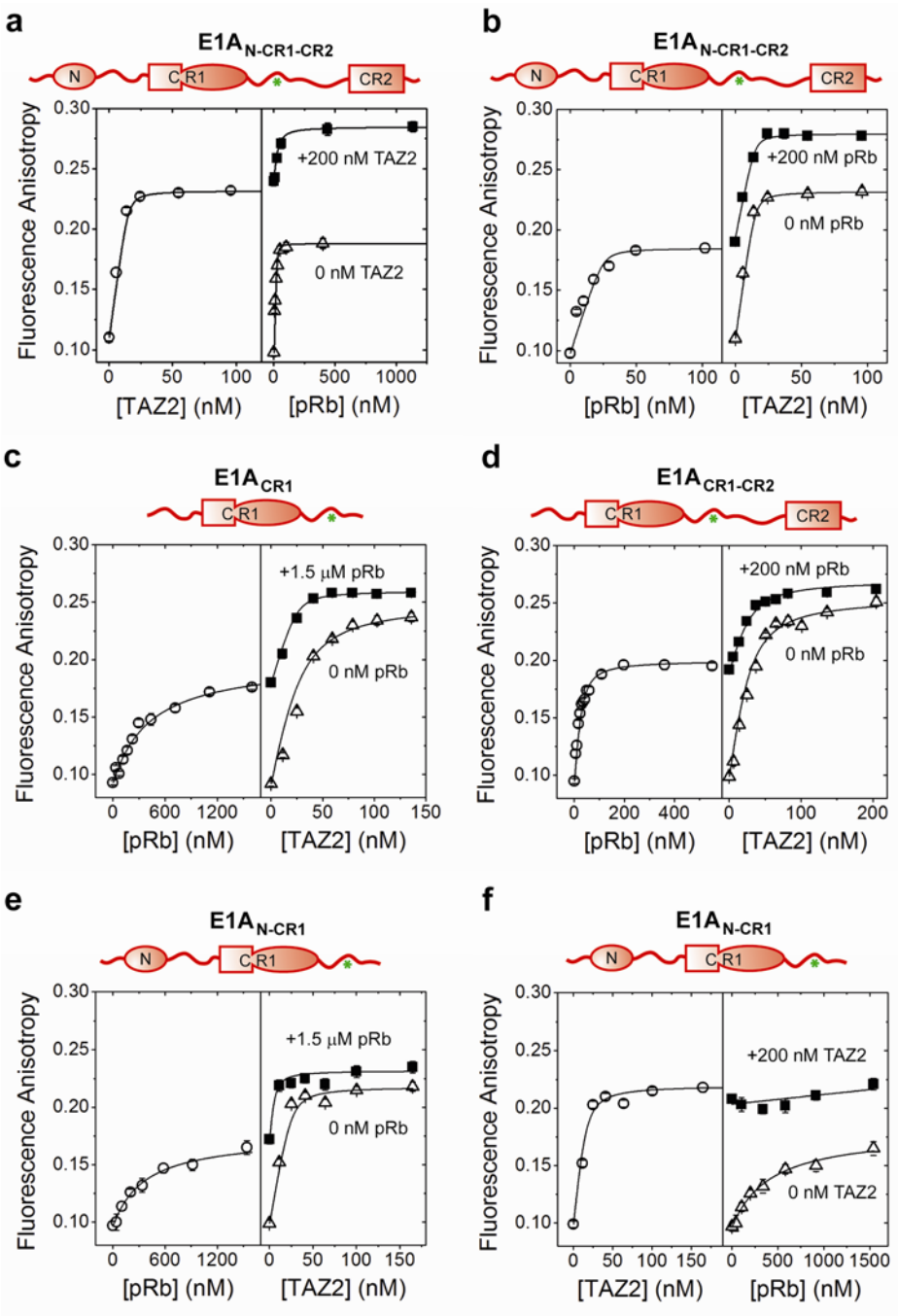

Supplementary Figure 1│ E1A-TAZ2-pRb ternary complex formation monitored using ensemble fluorescence anisotropy. Presented in **a-f** are titration data on the TAZ2/pRb binding of free (open symbols) and TAZ2- or pRb-bound (solid symbols) Alexa Fluor 594-labeled E1A. The specific E1A (S88C) constructs used are indicated. See Fig. 1b and Methods for more details.

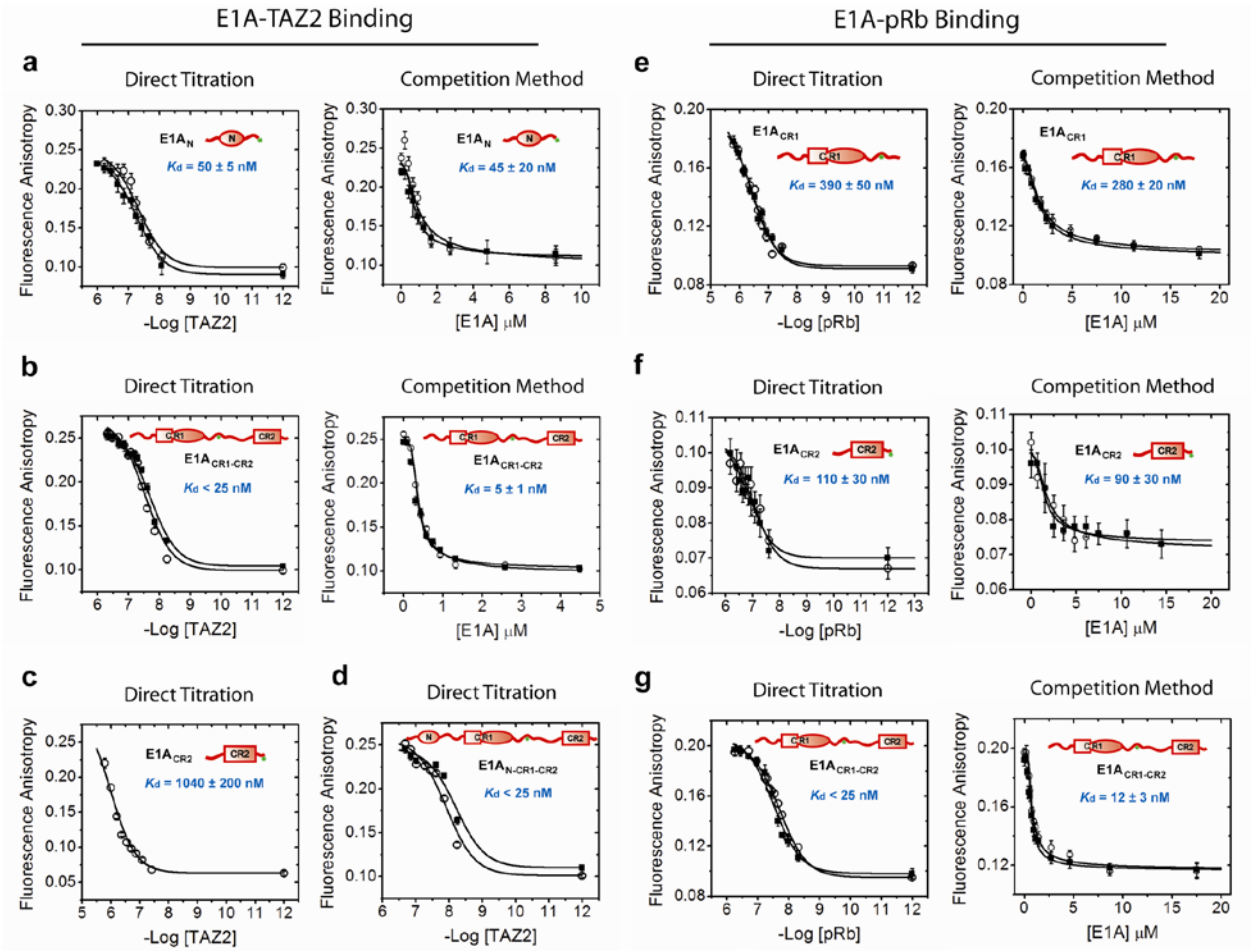

Supplementary Figure 2 | Determination of dissociation constants using ensemble fluorescence anisotropy. Shown are representative titration data on the TAZ2 (**a-d**) and pRb (**e-g**) binding of different Alexa Fluor 594-labeled E1A constructs using direct and competition methods. The specific E1A constructs used are indicated. See Fig. 1b and Methods for more details.

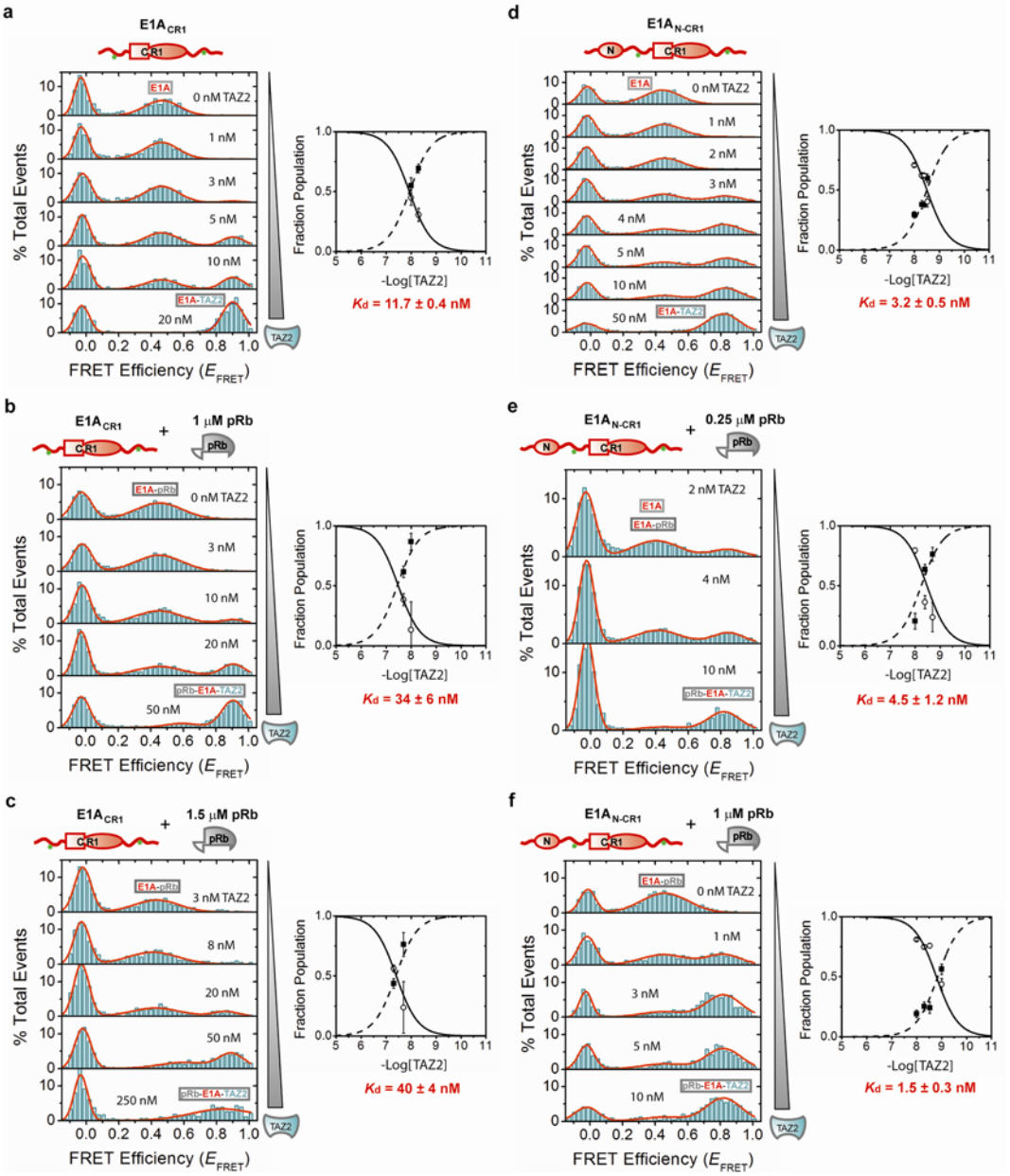

Supplementary Figure 3 | Determination of dissociation constants using smFRET: Allosteric interaction between the E1A N-terminal and CR1 regions. Shown are representative smFRET titration data of E1A$_{CR1}$(27-105; 36C88C) and E1A$_{N-CR1}$(1-105; 36C88C) with CBP TAZ2 in the absence (**a**,**d**) and presence of pRb (**b-c**, **e-f**). The concentration of pRb in the solution and the specific E1A FRET constructs used are indicated. Also shown for each set of titration data are the NLS best-fit curves to a one-to-one binding model for the ligand concentration dependence of the measured fractional populations (*i.e.*, fraction bound [open symbols] and unbound [filled symbols]), and the derived average K_d values and fitting errors. See Fig. 1b and Methods for more details.

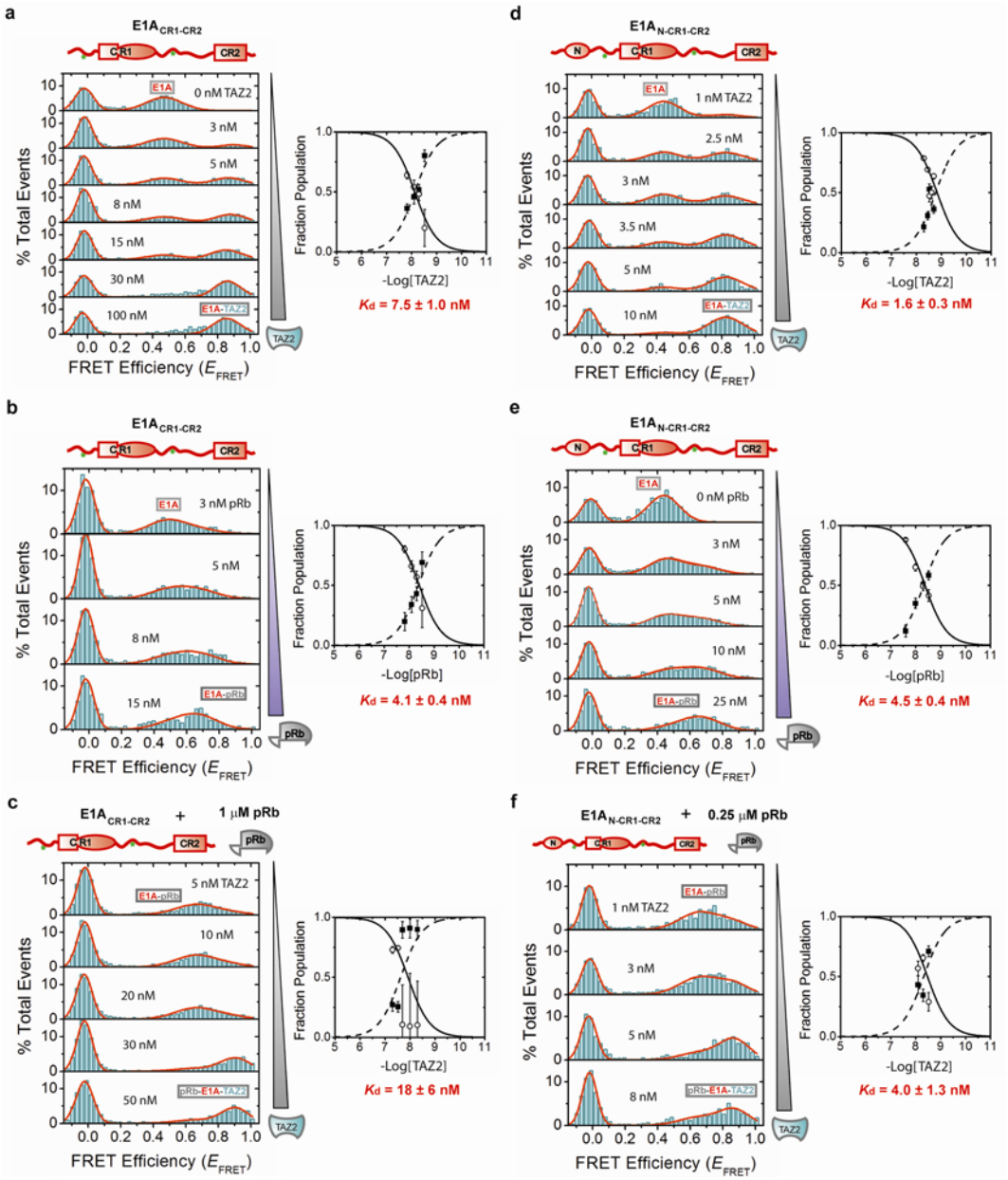

Supplementary Figure 4 | Determination of dissociation constants using smFRET: Allosteric interaction between the E1A N-terminal and CR1-CR2 regions (I). Shown are representative smFRET titration data of $E1A_{CR1-CR2}$(27-139; 36C88C) and $E1A_{N-CR1-CR2}$(1-139; 36C88C) with CBP TAZ2 (**a**, **c-d**, **f**) or pRb (**b**, **e**) in the absence (**a-b**, **d-e**) and presence of pRb (**c**, **f**) before titration. The pre-titration concentration of pRb (for **c** and **f**) and the specific E1A FRET constructs used are indicated. Also shown for each set of titration data are the NLS best-fit curves to a one-to-one binding model for the ligand concentration dependence of the measured fractional populations, and the derived average K_d values and fitting errors. See Fig. 1b and Methods for more details.

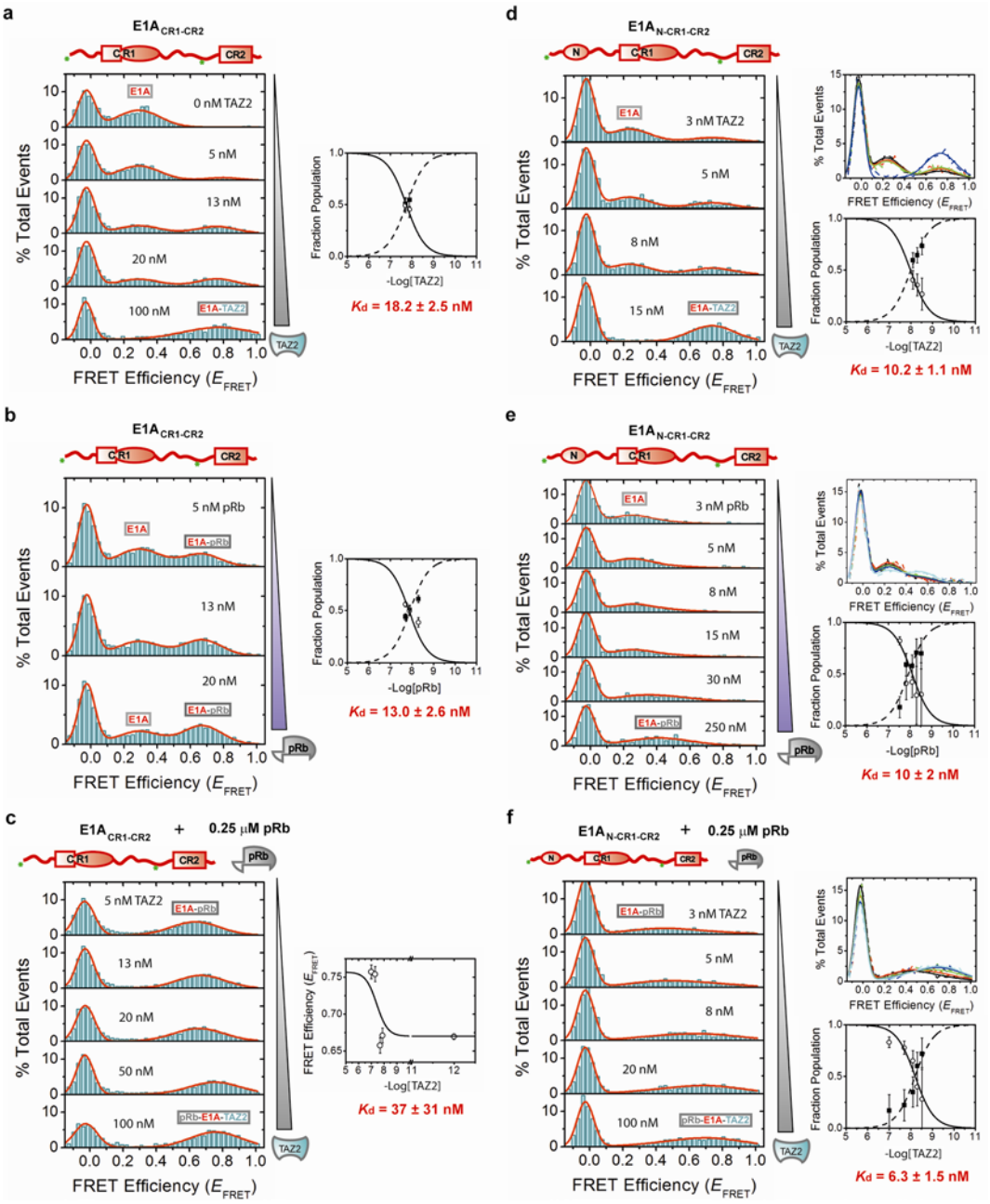

Supplementary Figure 5 | Determination of dissociation constants using smFRET: Allosteric interaction between the E1A N-terminal and CR1-CR2 regions (II). Shown are representative smFRET titration data of $E1A_{CR1-CR2}$(27-139; **-3C111C**) and $E1A_{N-CR1-CR2}$(1-139; **-3C111C**) with CBP TAZ2 (**a**, **c-d**, **f**) or pRb (**b**, **e**) in the absence (**a-b**, **d-e**) and presence of pRb (**c**, **f**) before titration. The pre-titration concentration of pRb (for **c** and **f**) and the specific E1A FRET constructs used are indicated. Also shown for each set of titration data are the NLS best-fit curves to a one-to-one binding model for the ligand concentration dependence of the measured fractional populations (**a-b**, **d-f**) or FRET efficiencies (**c**), and the derived average K_d values and fitting errors. See Fig. 1b and Methods for more details.

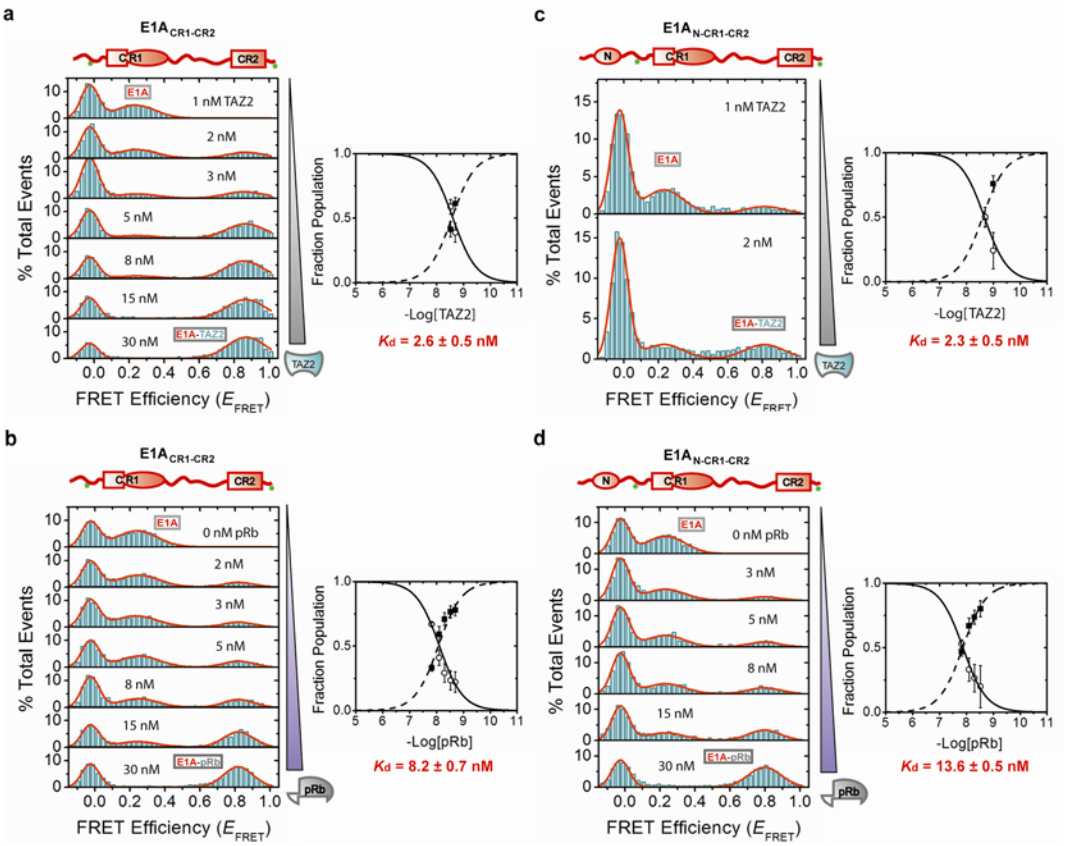

Supplementary Figure 6 | Determination of dissociation constants using smFRET: Allosteric interaction between the E1A N-terminal and CR1-CR2 regions (III). Shown are representative smFRET titration data of $E1A_{CR1\text{-}CR2}$(27-139; 36C137C) and $E1A_{N\text{-}CR1\text{-}CR2}$(1-139; 36C137C) with CBP TAZ2 (**a**, **c**) or pRb (**b**, **d**). The specific E1A FRET constructs used are indicated. Also shown for each set of titration data are the NLS best-fit curves to a one-to-one binding model for the ligand concentration dependence of the measured fractional populations, and the derived average K_d values and fitting errors. See Fig. 1b and Methods for more details.

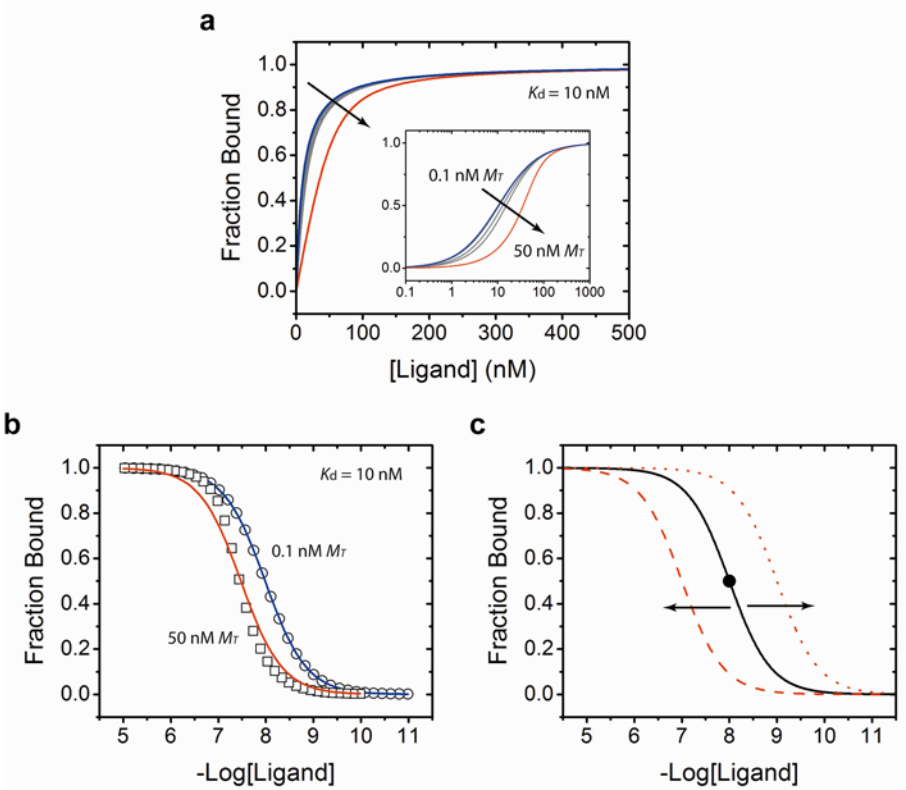

Supplementary Figure 7 | Ligand binding simulations. (**a**) The effect of the macromolecule concentration on ligand binding measurements. Data simulations were carried out using Eq. 3 (Methods), using fraction bound as observable, and assuming a K_d of 10 nM and macromolecule concentrations (M_T) of 0.1, 1, 5, 10 and 50 nM. M_T/K_d ratios of 1 or less result in binding curves that are practically identical. (**b**) Comparison of binding curves with different M_T/K_d ratios (0.01 vs. 5). The simulated data were fitted to Eq. 2 (Methods), assuming that the total ligand and free ligand concentrations are equal. This approximation is reasonably acceptable when the M_T/K_d ratio is small, as is the case with the smFRET experiments described in this paper (where M_T = 100 pM and the measured K_d values are all within the nM range; see Supplementary Table 2). When $M_T >> K_d$, the approximation becomes invalid and the application of Eq. 2, inappropriate. (**c**) Single-parameter model fitting. Because the binding stoichiometries are known, and given that the M_T/K_d ratios are small and the intercepts/slopes for the binding curves are constants (which is the case when using fraction populations as observable), single-parameter fits can be performed in the analyses of the smFRET binding data reported here. Thus, in principle, a single point within the binding transition is enough to determine K_d values using smFRET data, and the fitting process can be visualized and performed by horizontally "sliding" a bounded curve until it coincides with the data point.